Research Square

Preprints are preliminary reports that have not undergone peer review.
They should not be considered conclusive, used to inform clinical practice,
or referenced by the media as validated information.

Heterogeneously Integrated GaAsSb/Si Separate Absorption, Charge, and Multiplication (SACM) Photodiodes with Electrically Active Bonded Interface

Manisha Muduli
The Ohio State University
Sophie Mills
The Ohio State University
Dylan Plouffe
The Ohio State University
Nathan Gajowski
The Ohio State University
Punam Murkute
The Ohio State University
Yongkang Xia
The Ohio State University
Fritz Kyser
The Ohio State University
Shamsul Arafin
The Ohio State University
Sanjay Krishna
krishna.53@osu.edu

The Ohio State University

Article

Keywords: Heterogeneous integration, SACM, SWIR, transfer printing, EQE, gain

Posted Date: November 25th, 2026

DOI: https://doi.org/10.21203/rs.3.rs-11654294/v1

License: This work is licensed under a Creative Commons Attribution 4.0 International License.
Read Full License

Additional Declarations: No competing interests reported.

Heterogeneously Integrated GaAsSb/Si Separate Absorption, Charge, and Multiplication (SACM) Photodiodes with Electrically Active Bonded Interface

Manisha Muduli[1], Sophie Mills[1], Dylan Plouffe[1], Nathan Gajowski[1], Punam Murkute[1], Yongkang Xia[1], Fritz Kyser[1], Shamsul Arafin[1], Sanjay Krishna[1]*

[1]Department of Electrical and Computer Engineering, The Ohio State University, Columbus, OH 43201, USA
*Corresponding author: krishna.53@osu.edu

Keywords: Heterogeneous integration, SACM, SWIR, transfer printing, EQE, gain

Abstract:

Silicon photodetectors are limited to wavelengths below ~1100 nm, motivating heterogeneous integration of III-V absorbers for short-wave infrared (SWIR) detection. However, carrier transport across bonded III-V/Si heterointerfaces remains challenging due to interfacial defects and band discontinuities that can limit carrier injection into silicon avalanche photodiode architectures. Here, we demonstrate a transfer-printed GaAsSb/Si separate absorption, charge, and multiplication (SACM) photodiode with an electrically active bonded interface. Structural characterization reveals a void-free, compositionally abrupt heterointerface containing a thin interfacial oxide, while capacitance- and temperature-dependent measurements reveal electrically active interface states and bias-dependent carrier transport. Depletion analysis shows that the depletion region progresses through the Si structure and reaches the GaAsSb/Si heterointerface near punch-through, enabling carrier collection from the GaAsSb absorber. The photoresponse increases substantially with reverse bias, reaching an effective external quantum efficiency of 1079.8% at 1550 nm and −20 V, while the enhanced photoresponse results in improved noise-equivalent power at higher reverse bias. These results establish an electrically functional interface between a SWIR-absorbing III-V layer and a Si SACM structure, providing a pathway toward heterogeneously integrated III-V/Si avalanche photodiodes.

Introduction:

Many of the most critical innovations made within the semiconductor microelectronic ecosystem over the past 70 years have relied on the precise engineering of the “humble” Si/SiO2 interface. However, new

paradigms for “More than Moore” and “Beyond Moore” technologies[1], as well as advances across the even broader world of electronics and photonics outside of computing, increasingly rely on the integration of an ever-expanding palette of semiconductor and otherwise functional (quantum, magnetic, ferroelectric, dielectric, etc.) materials, and with that, increasingly complex interfaces[1]. As such, the need for recursive co-design of integrated materials, devices, and systems to enable new functionalities and applications is now more important than ever. Nowhere is this more obvious than in the rapidly emerging field of Si-integrated photonics for high-speed, high-efficiency on-chip/chip-to-chip optical communications needed to supplant legacy copper interconnects[2]. Advances in this area are critical to address urgent needs for bandwidth scaling (for aggregate densities beyond 1 Tbps/mm2), power consumption reduction (by ≥10× to stem the currently unsustainable growth trends), and per-bit costs (by ≥10× to ensure economic feasibility and accessibility). To satisfy these requirements, high-performance, Si-compatible optical I/O components – emitters (lasers or LEDs), modulators, receivers/photodetectors – must be developed.

Short-wave infrared (SWIR) photodiodes operating near the 1550 nm telecommunication window are essential for applications including optical communications, single-photon detection, LiDAR, remote sensing, and low-light imaging[3-7]. Many of these systems require high-sensitivity photodetection under weak optical signals, motivating the development of photodiodes with high quantum efficiency, low noise, and high internal gain[5-7]. Separate absorption, charge, and multiplication (SACM) architectures are particularly attractive because absorption and multiplication can be independently engineered to combine efficient photocarrier generation with internal gain while controlling excess noise.

InGaAs-based APDs remain the dominant SWIR detector technology because of their strong absorption near 1550 nm and mature device performance[8,9]. However, these devices can exhibit substantial band discontinuities at the heterojunction interface, complicating efficient carrier transfer from the InGaAs absorber into the Si multiplication region. Ge/Si photodiodes offer compatibility with silicon integration, but typically suffer from elevated dark current and reduced SWIR performance[10]. These limitations

motivate the exploration of heterogeneously integrated III-V/Si SACM photodiodes that combine efficient III-V absorption with low-noise Si multiplication[11-13].

Although heterogeneous III-V/Si photodiodes have been widely explored[13-16], efficient carrier transfer into Si multiplication regions remains fundamentally challenging due to the bonded heterojunction interface. Electrically active interface states, interfacial oxides, and band-offset discontinuities can impede carrier transport across the heterojunction, particularly under reverse bias, where photogenerated carriers must efficiently traverse the interface and inject into the Si multiplication region[16]. Consequently, the performance of heterogeneously integrated SACM photodiodes depends critically on efficient carrier transport between the III-V absorber and Si multiplication region.

GaAsSb is particularly attractive for heterogeneously integrated SWIR photodiodes because of its favorable conduction-band alignment with Si[17-20], which enables efficient carrier transfer across the heterojunction interface. Additionally, GaAsSb's absorption and quantum efficiency near 1550 nm is comparable to that of InGaAs, the benchmark for SWIR technologies[21].

In this work, we demonstrate a heterogeneously integrated GaAsSb/Si SACM photodiode fabricated by micro transfer-printing a GaAsSb absorber onto a silicon charge and multiplication structure, as shown in Fig. 1(a), with the corresponding microscope images shown in Fig. 1(b). In the designed SACM structure, GaAsSb serves as the 1550 nm absorber, while Si serves as the charge and multiplier, forming the core architecture of a heterogeneously integrated avalanche photodiode (APD). A schematic of the final device structure shown in Fig. 1 (c). Silvaco simulations reveal a favorable conduction band alignment between GaAsSb and Si (Fig. 1 (d), supporting carrier transport hypothesis across the GaAsSb/Si interface.

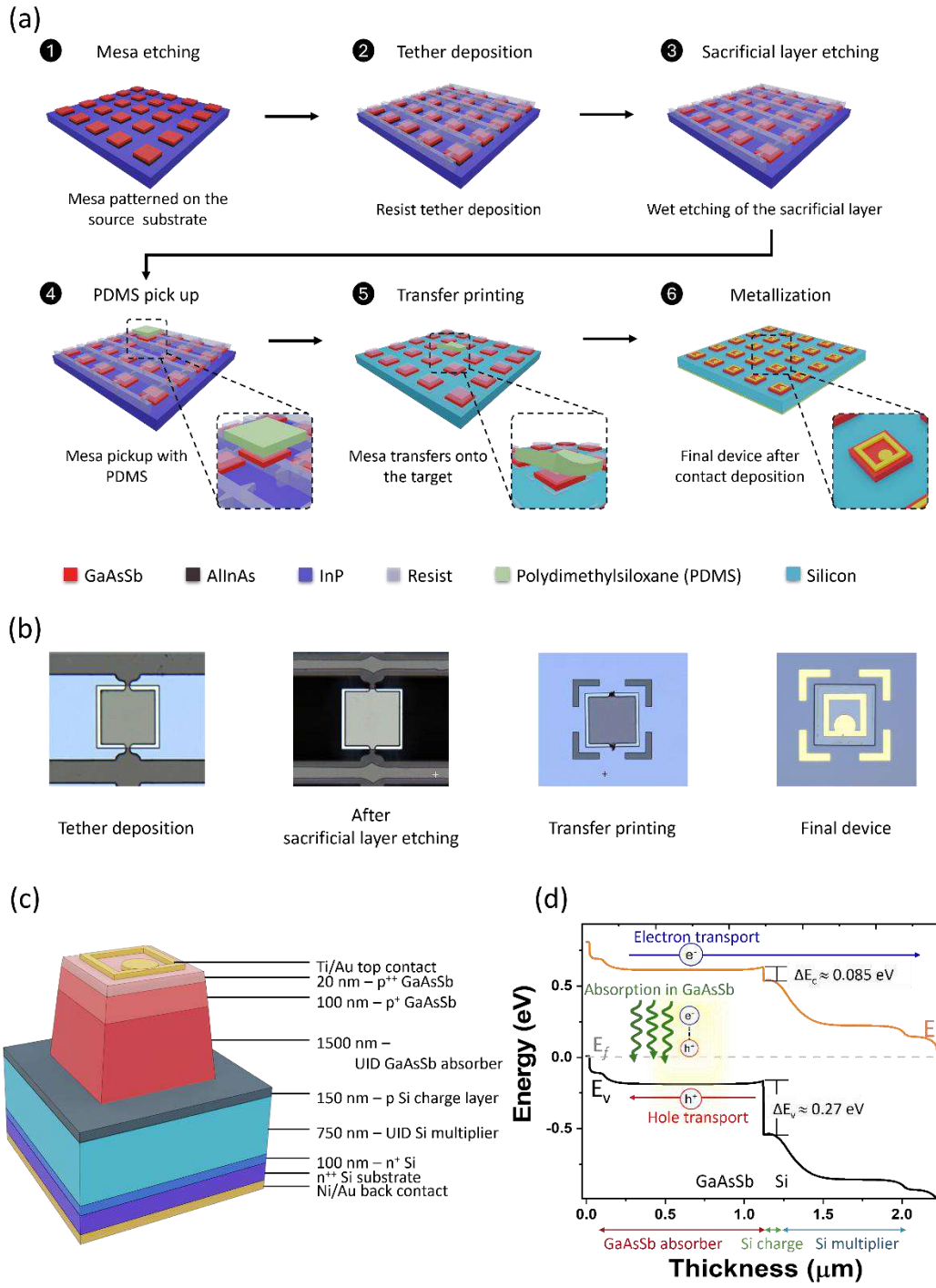

Fig. 1 Process outline and band alignment simulation. (a) (1-6) Process sequence showing mesa formation, tether deposition, separation of epi via sacrificial layer etching, mesa pickup using PDMS, micro transfer printed mesa onto Si, and metallization of the final device. Insets: highlight key structural features during processing. (b) Optical microscope images of devices during different processing steps. (c) The epitaxial cross-section of the final device consisting of a transfer-printed GaAsSb absorber layer on top of a Si multiplier. (d) The simulated energy band diagrams for the device at equilibrium.

Structural characterization of the transfer-printed GaAsSb/Si heterostructure confirms a high-quality, continuous and void-free interface between GaAsSb and Si. Temperature-dependent transport and capacitance measurements reveal electrically active interface states and provide insight into the carrier transport across the heterostructure. Bias-dependent depletion and photoresponse measurements demonstrate carrier collection from the GaAsSb absorber, with the device reaching an effective external quantum efficiency exceeding 1000% under 1550 nm illumination

Results:

SEM and EDS Analysis: A cross-sectional scanning electron microscopy (SEM) image of the transfer-printed device reveals a continuous and void-free bonded interface between the GaAsSb epilayer and the Si substrate, confirming successful heterogeneous integration and robust interfacial adhesion (Fig. 2 (a)). High-angle annular dark-field scanning transmission electron microscopy (HAADF-STEM) shown in Fig. 2 (b) further shows a structurally abrupt and laterally uniform GaAsSb/Si heterojunction interface without observable interfacial voids or delamination. Corresponding energy-dispersive X-ray spectroscopy (EDS) elemental maps demonstrate strong spatial confinement of Ga, As, and Sb within the GaAsSb absorber layer, while Si remains localized within the substrate. The abrupt structural and compositional transitions at the interface indicate negligible interdiffusion between the GaAsSb and Si regions.

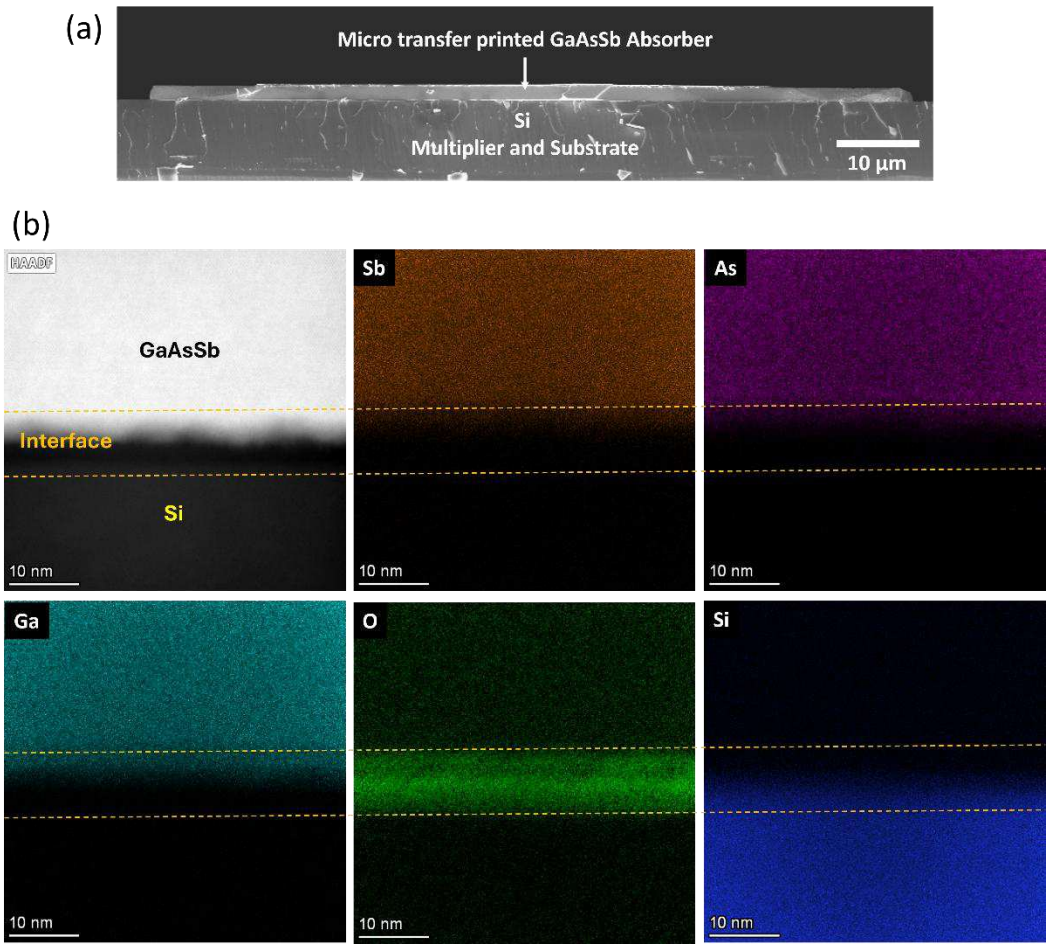

Fig. 2 Structural characterization of the transfer-printed GaAsSb/Si heterojunction interface. (a) Cross-sectional SEM image of the GaAsSb/Si SACM photodiode showing a continuous and void-free bonded interface between the GaAsSb absorber and Si multiplication regions. (b) HAADF-STEM image and corresponding EDS elemental maps of the GaAsSb/Si heterojunction interface. The yellow lines define the interface by the oxygen-rich interfacial layer.

In contrast, the oxygen map shows continuous enrichment at the bonded interface, consistent with a thin amorphous interfacial oxide layer. This oxygen-rich region likely originates from residual native oxides on the GaAsSb and Si surfaces prior to bonding. Although oxides are usually detrimental to device performance, it is observed that such ultrathin native oxides can also improve interfacial adhesion and bonding uniformity during heterogeneous integration[20,22]. The electrical consequences of this interfacial oxide are examined through the capacitance and transport measurements discussed below.

Capacitance-voltage and effective trap density: Fig. 3 (a) shows the capacitance-voltage (CV) characteristics measured under dark conditions and under 1550 nm illumination. At low reverse bias, the

device exhibits increased capacitance under illumination compared to dark conditions, indicating photogenerated carrier accumulation and charge modulation near the GaAsSb/Si heterojunction interface[16]. This behavior is consistent with electrically active interface states that influence photocarrier accumulation and collection near the bonded interface junction under low electric fields. As the reverse bias increases, the illuminated and dark capacitance characteristics gradually converge, while minor fluctuations are observed in the illuminated C-V response. These minor fluctuations suggest active generation and recombination in the detector, with recombination potentially arising from interface defects or oxide trap states[23,24].

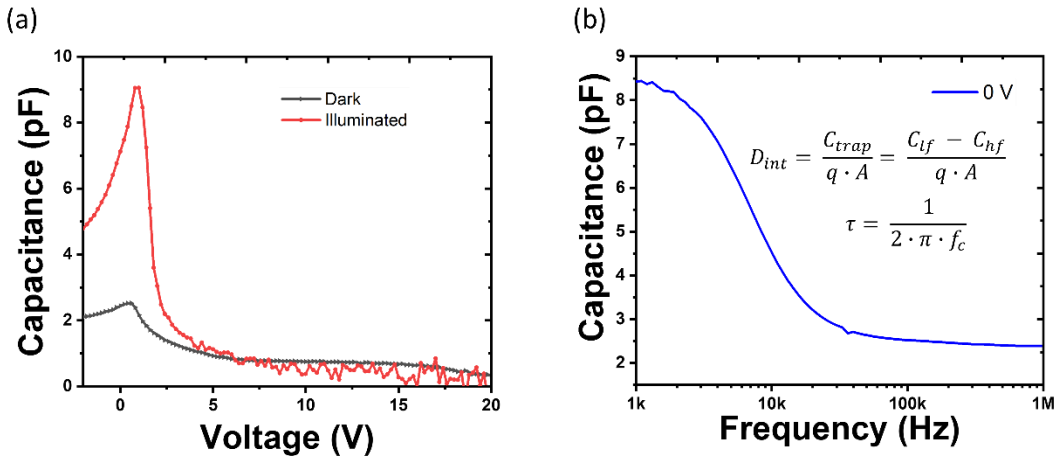

Fig. 3 Capacitance characterization of interface-mediated carrier transport in the GaAsSb/Si SACM heterojunction. (a) CV characteristics measured under dark and illuminated conditions at 1Mhz frequency. (b) Cf measurement under dark conditions at 0 V bias. (Inset) D_{int} is the effective interface trap density, C_{lf} low frequency capacitance, C_{hf} high frequency capacitance, A is the area of the device, τ is the trap response time, f_c is the roll-off frequency.

Using the capacitance-frequency (Cf) response shown in Fig. 3b, the effective interface trap density is estimated to be $5.2 \times 10^{11}\ \mathrm{cm}^{-2}$, using the high-low frequency (Castagné–Vapaille) method[25,26]. The corresponding trap response time is estimated to be 19 μs using the equation in Fig. 3[26,27]. The observed capacitance-voltage response and relatively slow trap response dynamics indicate the presence of electrically active interface states that can modulate local electric-field distribution and carrier transport across the heterojunction. These measurements establish the presence of electrically active states at the bonded GaAsSb/Si interface that can influence carrier transport within the heterostructure.

Current-voltage, and carrier transport mechanism: The room-temperature dark and illuminated current-density characteristics of the GaAsSb/Si SACM photodiode is shown in Fig. 4 (a). The relatively small GaAsSb/Si conduction-band offset (simulated value: 0.085 eV; reported value: ~0.05 eV)[17] enables efficient injection of photogenerated carriers from the GaAsSb absorber into the Si multiplication region, including at relatively low reverse bias. The presence of photocurrent under 1550 nm illumination at low reverse bias indicates that photogenerated carriers can be collected from the GaAsSb absorber even before the depletion region reaches the GaAsSb/Si heterointerface. As the reverse bias increases, the depletion region extends through the Si structure and reaches the GaAsSb/Si heterointerface at approximately −6 V, after which it progressively extends into the GaAsSb absorber. Since the depletion region does not reach the GaAsSb/Si heterointerface until approximately −6 V, the low-bias photocurrent cannot be assumed to represent complete carrier collection or a unity-multiplication condition. Hence, an absolute avalanche multiplication factor is not extracted from the photocurrent characteristics.

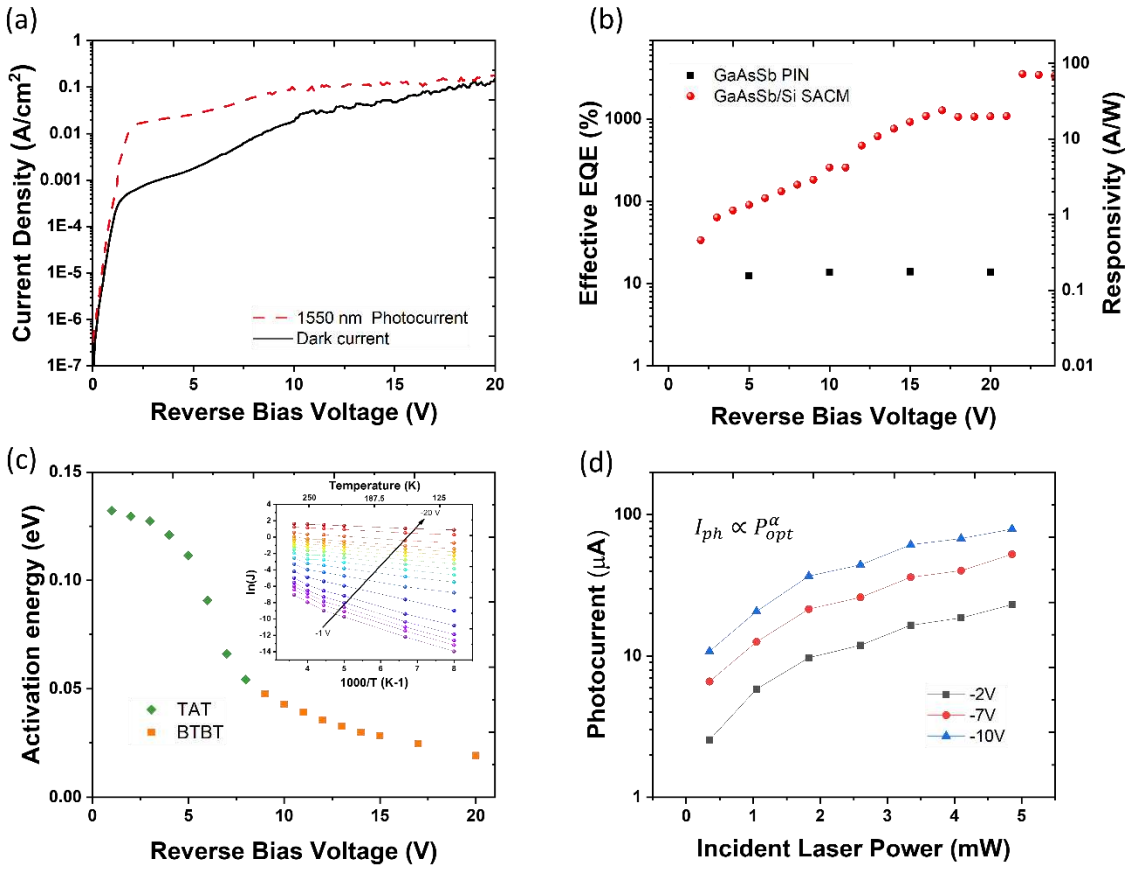

Fig. 4 Electrical characterization and transport mechanism of the GaAsSb/Si SACM photodiode. (a) Photocurrent and dark current characteristics of the diode at room temperature with applied bias. (b) External quantum efficiency and responsivity of GaAsSb/Si SACM and GaAsSb PIN diode. (c) Extracted activation energy as a function of reverse bias, showing a transition from thermally activated transport to tunneling-dominated conduction at high electric fields. (inset) Arrhenius plots of ln(J) versus 1000/T at different reverse biases used to extract activation energies and identify dominant transport mechanisms; TAT: Trap-Assisted Tunneling, BTBT: Band-to-Band Tunneling. (d) Photocurrent as a function of incident laser power of the GaAsSb/Si SACM.

The *effective* external quantum efficiency (EQE) of the GaAsSb/Si SACM and the GaAsSb PIN diode are shown in Fig. 4 (b). Fabrication details for the PIN reference device are provided in Supplementary Section 1.1. The GaAsSb PIN photodiode exhibits an EQE of 13.8% at −20 V and 13.86% at −22 V. In comparison, the GaAsSb/Si SACM photodiode achieves effective EQE of 1079.8% at -20 V, increasing to3538% at −22 V. At −20 V, this corresponds to about 78x enhancement in effective EQE compared with the GaAsSb PIN reference device. The effective EQE exceeding 100% demonstrates internal gain within the heterostructure; however, the present measurements do not independently separate avalanche multiplication from the bias-dependent enhancement in carrier collection. The substantial increase in effective EQE after the depletion region reaches the GaAsSb/Si heterointerface is consistent with enhanced photocarrier collection and internal gain at higher reverse bias.

Activation energy extracted from the Arrhenius analysis is shown in Fig. 4 (c). The activation energy decreases continuously from approximately 0.15 eV at low reverse bias to below 0.03 eV at high reverse bias, accompanied by progressively weaker temperature dependence under increasing electric field. At low reverse bias, when the depletion region is confined to the Si layer, the extracted activation energy is relatively high (0.15 eV), consistent with thermally activated carrier transport over the GaAsSb/Si heterointerface barrier. As the reverse bias increases, the decreasing activation energy indicates a reduced contribution from thermally activated transport, while the Poole-Frenkel behavior (Supplementary Figure 10. (c)) at intermediate fields is consistent with field-assisted emission from electrically active trap states. At high reverse bias, the activation energy falls below the simulated GaAsSb/Si conduction-band offset, while the observed Fowler-Nordheim behavior (Supplementary Figure 10. (d)) is consistent with an increasing contribution from field-induced tunneling to carrier transport.

The transport behavior is further analyzed using the power law for photoresponse of diodes[28,29]. The power-dependent photoresponse of the GaAsSb/Si SACM diode is shown in in Fig. 4 (d). The photocurrent (I_{ph}) scales sublinearly with incident optical power (P_{opt}) according to $I_{ph} \propto P_{opt}^{\alpha}$, with a power-law exponent of $\alpha \approx 0.77$. The sublinear power dependence and the exponent of $\alpha \approx 0.77$ are consistent with trap-mediated recombination and carrier-collection effects within the detector. Together with the capacitance and temperature-dependent transport analysis, these defects likely arise from the electrically active trap states at the GaAsSb/Si heterointerface.

Radiometric characterization: The measured noise current (I_{noise}) as a function of reverse bias for the GaAsSb/Si SACM detector and the GaAsSb PIN diode is shown in Fig. 5 (a). The PIN diode exhibits relatively weak bias dependence in noise current across the measured voltage range. In contrast, the GaAsSb/Si SACM device exhibits a progressive increase in noise current with increasing reverse bias, coincident with the increase in dark current and photoresponse at higher electric fields. This bias-dependent noise response is consistent with the evolving carrier transport and electric-field distribution within the SACM heterostructure. The measured noise represents the total noise under the experimental measurement conditions, and the individual contributions from dark-current noise, trap-related noise, and gain-related noise are not independently separated.

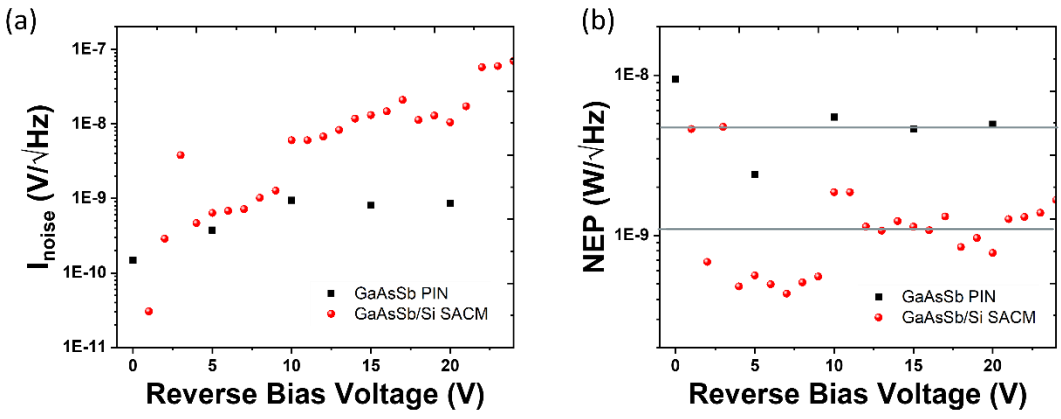

Fig. 5 Radiometric characterization and device performance. (a) Dark noise, (b) Noise-equivalent power (NEP) characteristics of GaAsSb/Si SACM and GaAsSb PIN diodes of the GaAsSb/Si SACM diode.

Figure 5 (b) compares the noise-equivalent power (NEP) characteristics of the PIN GaAsSb diode and the transfer-printed GaAsSb/Si SACM device. The PIN diode exhibits a nearly bias-independent NEP of approximately $4 \times 10^{-9}\,\mathrm{W\,Hz^{-1/2}}$, consistent with its relatively weak bias dependence of the responsivity and the measured I_{noise}. By comparison, the GaAsSb/Si SACM device achieves a lower NEP of approximately $1 \times 10^{-9}\,\mathrm{W\,Hz^{-1/2}}$ at higher bias, as the enhancement in photoresponse outweighs the accompanying increase in measured noise current. The GaAsSb/Si SACM diode yielded a calculated shot-noise-limiteddetectivity (D*) of $\sim 9 \times 10^{11}$ Jones at -17 V, assuming dark-current shot noise as the limiting noise contribution[30]. These results demonstrate that the enhanced photoresponse of the transfer-printed GaAsSb/Si SACM architecture can improve SWIR detection sensitivity despite the accompanying increase in measured noise at higher reverse bias.

Discussion: Table 1 compares the performance of the transfer-printed GaAsSb/Si SACM photodiode with previously reported heterogeneously integrated III-V/Si photodetectors operating near 1550 nm. The comparison includes the dark current at punchthrough voltage (V_{pt}), unity-gain responsivity, maximum effective quantum efficiency (QE), and gain. While many previously reported III-V/Si photodetectors rely on heterogeneous integration of III-V photodiodes onto silicon waveguide platforms, the present architecture instead integrates a GaAsSb absorber directly onto a Si charge and multiplication region to enabling carrier injection across the bonded heterojunction interface.

Table 1 Comparison of GaAsSb/Si SACM diode (this work) with other emerging III-V/Si detectors.

Absorption/ Multiplication Region	**Integration Type**	I_{dark} **at** V_{pt}	**Unity-Gain** R **(A/W)**	**Max effective** QE **/ Gain**
GaAsSb/Si (This work)	Integration of GaAsSb absorber on Si multiplier	42 nA	1.37* *(at* V_{pt}*)*	1079.8% (at -20 V) / -
InGaAs/InP[31]	Heterogeneous integration of diode on a waveguide	5 nA	0.61	49% / 166

InGaAs/InAlGaAs[32]	Heteroepitaxy of diode on a waveguide	200 nA	0.27	—
InGaAs/InP[33]	Heterogeneous integration of diode on a waveguide	2 nA	0.22	18% / —
InGaAs/InAlAs[34]	Heteroepitaxy of diode on a waveguide	9 nA	0.54	— / 20
InGaAs/InAlAs[35]	Heterogeneous integration of diode on a waveguide	~ 10 nA	0.39	57% / 100

*Since the unity-gain condition was not independently determined in this work, the responsivity at the punch-through voltage is reported for comparison, as the unity-gain condition in SACM photodiodes is typically established near or above punch-through.

The GaAsSb/Si SACM device exhibits a higher dark current than several previously reported heterogeneous III-V/Si photodiodes. This behavior is attributed primarily to electrically active interface states and surface leakage which can arise with the current unpassivated device geometry. With further optimization of the GaAsSb/Si SACM diode, this dark current can be reduced using surface passivants and engineering the GaAsSb/Si heterointerface. Despite the increased dark current, the device achieves high EQE values comparable to state-of-the-art heterogeneous III-V/Si photodetectors at room temperature. The effective EQE exceeding 100% provides evidence of internal gain in the GaAsSb/Si SACM photodiode, although the absolute avalanche multiplication factor cannot be independently determined from the present measurements.

Although further optimization of interface quality, surface passivation, and device design will be necessary to reduce dark current and clarify the avalanche multiplication characteristics of the GaAsSb/Si platform, these results demonstrate the strong potential of transfer-printed GaAsSb/Si SACM photodiodes for silicon-integrated SWIR detection. These results highlight GaAsSb/Si heterointerface engineering as an effective strategy for controlling carrier transport between the III-V absorber and Si charge and multiplication regions. More broadly, this work demonstrates a pathway for integrating SWIR-sensitive III-V absorbers

with Si SACM structures without requiring the absorber and multiplication regions to share a common epitaxial material system. The transfer-printing approach may therefore be extended to other III-V absorber compositions and heterogeneous III-V/Si photodetector architectures.

Conclusion:

In summary, we demonstrated a transfer-printed GaAsSb/Si SACM photodiode integrating a GaAsSb SWIR absorber with Si charge and multiplication regions through a bonded heterointerface. Structural characterization revealed a void-free, compositionally abrupt GaAsSb/Si interface while capacitance- and temperature-dependent measurements revealed electrically active interface states that participate in carrier transport and electric-field redistribution. Bias-dependent depletion analysis shows that the depletion region progresses through the Si structure, reaches the GaAsSb/Si heterointerface near punch-through, and subsequently extends into the GaAsSb absorber. The favorable conduction-band alignment, together with the observed 1550 nm photocurrent, supports photocarrier transport from the GaAsSb absorber across the bonded heterointerface into the Si SACM structure. The device achieves an effective EQE exceeding 1000% at −20 V, providing evidence of internal gain, while the enhanced photoresponse at higher reverse bias results in improved noise-equivalent power relative to a GaAsSb PIN reference device. These results demonstrate the potential of transfer-printed III-V/Si SACM photodiodes to combine the strong SWIR absorption of III-V semiconductors with Si-based charge and multiplication structures, highlighting the importance of electrically functional bonded heterointerfaces in heterogeneous photodetector integration.

Methods:

Device Fabrication:

The fabrication process for the transfer-printed GaAsSb photodetector devices is illustrated in Fig. 1 (a) and comprises six major steps: mesa definition, tether formation, sacrificial layer release, PDMS-assisted pickup, transfer printing, and contact deposition.

First, high-quality, lattice-matched GaAsSb was epitaxially grown on an InP substrate with an AlInAs sacrificial layer, using molecular beam epitaxy (MBE). The epitaxially grown epi was patterned using standard photolithography followed by reactive ion etching (RIE). The mesa structures were defined to expose the surrounding sacrificial layer while maintaining the active device geometry, as shown in Step 1 of Fig. 2(a).

Next, a SPR220 resist was spin-coated and patterned to form the tether structure around each mesa (Step 2). These tethers hold the defined mesas in place and mechanically stabilize them during the sacrificial-layer etch and mesa-release processes. The sacrificial AlInAs layer beneath the mesas was then selectively removed using an HCl-based etchant. This undercut process partially suspended the mesas while leaving them connected through the resist tethers, thereby enabling controlled release.

After removal of the sacrificial layer, a polydimethylsiloxane (PDMS) stamp was brought into contact with the released mesas (Step 4). Due to PDMS's adhesion properties, the suspended mesas were mechanically lifted from the source substrate by fracturing the resist tether connections.

The mesas were then micro-transfer-printed onto the silicon target substrate, as illustrated in Step 5. For the target substrate, a lattice-matched PIN Si structure was separately grown on an n-Si substrate. Controlled alignment and pressure-assisted printing enabled the mesas to be accurately positioned on predefined locations of the silicon substrate. The mesas were initially transferred to the Si using Vanderwal’s forces. The adhesion between the mesas and the target substrate exceeded that between the mesas and the PDMS stamp, resulting in successful transfer. The transferred devices were cleaned with acetone and isopropanol to remove the residual resist. The stack was then annealed for 5 min at 300°C, which is below the growth temperature of GaAsSb. No surface passivation layer was deposited on these devices.

Finally, contact metal was deposited to complete the device fabrication (Step 6). Ti/Au was deposited on GaAsSb, and Ni/Au was deposited on Si to form ohmic contacts. The contact on the mesas isolated each mesa for individual testing, whereas the contact on Si acted as a common back contact.

The optical microscope images in Fig. 1(b) of the main paper further confirm the successful progression of the fabrication process, including tether formation, sacrificial layer release, transfer printing, and the final fabricated device, which shows an 85 μm device size.

Responsivity, Quantum Efficiency, and Noise Measurement Set-up:

The responsivity (R) and quantum efficiency (QE) measurements were obtained under 1550 nm illumination modulated at 313 Hz. The optical excitation was delivered through a 90/10 fiber splitter, where the calibrated 90% line measured 12 μW, and the underfilled 10% line was directed onto the device under test, delivering 1.33 uW. The RF dark noise and signal response of the devices were extracted through a Femto DHPCA-100 preamplifier to a Moku Lab spectrum analyzer using a Flat-Top window, 100 Hz span, 0.9327 Hz resolution bandwidth, and 0.230 Hz video filter to measure the power spectral density (V/√Hz).

Data availability:

The data that support the plots within this paper and other findings of this study are available from the corresponding authors upon reasonable request.

References:

1 Roelkens, G. *et al.* Integration of InP/InGaAsP photodetectors onto silicon-on-insulator waveguide circuits. *Optics Express* **13**, 10102-10108 (2005).

2 Miao, Y. *et al.* Review of Ge (GeSn) and InGaAs avalanche diodes operating in the SWIR spectral region. *Nanomaterials* **13**, 606 (2023).

3 Eng, P. C., Song, S. & Ping, B. State-of-the-art photodetectors for optoelectronic integration at telecommunication wavelength. *Nanophotonics* **4**, 277-302 (2015). https://doi.org/10.1515/nanoph-2015-0012

4 Beckerwerth, T., Runge, P. & Schell, M. High-Speed Photodiodes for Power Efficient Data Transmission. *Journal of Lightwave Technology* **42**, 1056-1061 (2024). https://doi.org/10.1109/jlt.2023.3322467

5 Rituraj, Yu, Z. G., Kandegedara, R. M. E. B., Fan, S. & Krishnamurthy, S. Highly sensitive and efficient 1550 nm photodetector for room temperature operation. *AIP Advances* **15** (2025). https://doi.org/10.1063/5.0238863

6 Lee, S. *et al.* High gain, low noise 1550 nm GaAsSb/AlGaAsSb avalanche photodiodes. *Optica* **10** (2023). https://doi.org/10.1364/optica.476963

7 Hadfield, R. H. *et al.* Single-photon detection for long-range imaging and sensing. *Optica* **10** (2023). https://doi.org/10.1364/optica.488853

8 Fang, Y.-Q. *et al.* InGaAs/InP single-photon detectors with 60% detection efficiency at 1550 nm. *Review of Scientific Instruments* **91** (2020). https://doi.org/10.1063/5.0014123

9 Signorelli, F. *et al.* in *2021 IEEE International Electron Devices Meeting (IEDM)* 20.23.21-20.23.24 (2021).

10 Lin, Y., Son, B., Lee, K. H., Michel, J. & Tan, C. S. Sub-mA/cm2 Dark Current Density, Buffer-Less Germanium (Ge) Photodiodes on a 200-mm Ge-on-Insulator Substrate. *IEEE Transactions on Electron Devices* **68**, 1730-1737 (2021). https://doi.org/10.1109/ted.2021.3061362

11 Kang, Y. *et al.* Fused InGaAs-Si avalanche photodiodes with low-noise performances. *IEEE Photonics Technology Letters* **14**, 1593-1595 (2002). https://doi.org/10.1109/lpt.2002.803370

12 Andresen, B. F. *et al.* in *Infrared Technology and Applications XXX* (2004).

13 Hawkins, A. R., Wu, W., Abraham, P., Streubel, K. & Bowers, J. E. High gain-bandwidth-product silicon heterointerface photodetector. *Applied Physics Letters* **70**, 303-305 (1997). https://doi.org/10.1063/1.118399

14 Liang, D. & Bowers, J. E. Recent Progress in Heterogeneous III-V-on-Silicon Photonic Integration. *Light: Advanced Manufacturing* **2** (2021). https://doi.org/10.37188/lam.2021.005

15 Liu, A. Y. & Bowers, J. Photonic integration with epitaxial III–V on silicon. *IEEE Journal of Selected Topics in Quantum Electronics* **24**, 1-12 (2018).

16 Xia, Y. *et al.* Investigation of the surface treatment of GaAsSb/Si using current– and capacitance–voltage measurements. *Journal of Applied Physics* **139** (2026). https://doi.org/10.1063/5.0316959

17 Abbasi, H. N. *et al.* Structural and electrical properties of grafted Si/GaAsSb heterojunction. *Applied Physics Letters* **125** (2024). https://doi.org/10.1063/5.0225069

18 Muduli, M. *et al.* Active interface characteristics of heterogeneously integrated GaAsSb/Si photodiodes. *Applied Physics Letters* **125** (2024). https://doi.org/10.1063/5.0230901

19 Nallamothu, N. S. *et al.* in *Optical Interconnects and Packaging 2025* (2025).

20 Nallamothu, N. S. *et al.* GaAsSb–silicon interface analysis for photodetectors via direct wafer bonding. *Optical Materials Express* **16** (2026). https://doi.org/10.1364/ome.578886

21 Jung, H. *et al.* High electric field characteristics of GaAsSb photodiodes on InP substrates. *Applied Physics Letters* **122** (2023). https://doi.org/10.1063/5.0154844

22 Plach, T. *et al.* Mechanisms for room temperature direct wafer bonding. *Journal of Applied Physics* **113** (2013). https://doi.org/10.1063/1.4794319

23 Lee, J. U. *et al.* Optical capacitance-voltage characterization of charge traps in the trapping nitride layer of charge trapped flash memory devices. *Applied Physics Letters* **91** (2007).

24 Chang, Y.-G., Lee, H. S., Choi, K. & Im, S. Capacitance–voltage measurement with photon probe to quantify the trap density of states in amorphous thin-film transistors. *IEEE electron device letters* **33**, 1015-1017 (2012).

25 Engel-Herbert, R., Hwang, Y. & Stemmer, S. Comparison of methods to quantify interface trap densities at dielectric/III-V semiconductor interfaces. *Journal of applied physics* **108** (2010).

26 Zhao, P. *et al.* Evaluation of border traps and interface traps in HfO2/MoS2 gate stacks by capacitance–voltage analysis. *2D Materials* **5**, 031002 (2018).

27 Zou, X. *et al.* Trap characterization techniques for GaN-Based HEMTs: A critical review. *Micromachines* **14**, 2044 (2023).

28 Shao, R. *et al.* in *2024 IEEE International Electron Devices Meeting (IEDM).* 1-4 (IEEE).

29 Zhao, Q. *et al.* The role of traps in the photocurrent generation mechanism in thin InSe photodetectors. *Materials horizons* **7**, 252-262 (2020).

30 Pecunia, V. *et al.* Guidelines for accurate evaluation of photodetectors based on emerging semiconductor technologies. *Nature Photonics*, 1-11 (2025).

31 Fatema, T. *et al.* Heterogeneously integrated waveguide-coupled InGaAs/InP SACM avalanche photodiodes on silicon nitride for 1550 nm. *Opt Express* **34**, 8787-8794 (2026). https://doi.org/10.1364/OE.587067

32 Gao, J., Sun, K., Jung, D., Bowers, J. & Beling, A. in *2020 Conference on Lasers and Electro-Optics (CLEO).* 1-2 (IEEE).

33 Jung, Y. *et al.* High-bandwidth InGaAs photodetectors heterogeneously integrated on silicon waveguides using optofluidic assembly. *Laser & Photonics Reviews* **16**, 2100306 (2022).

34 Yuan, Y. *et al.* Avalanche photodiodes on silicon photonics. *Journal of Semiconductors* **43** (2022). https://doi.org/10.1088/1674-4926/43/2/021301

35 Shao, R. *et al.* in *2024 IEEE International Electron Devices Meeting (IEDM)* 1-4 (2024).

Acknowledgements

The PIN Si was grown by Robin C. Scott from Lawrence Semiconductors, Tempe, Arizona.

Electron microscopy was performed at the Center for Electron Microscopy and Analysis (CEMAS) at The Ohio State University, Columbus, Ohio.

This work was supported by Intel's Center for Advanced Semiconductor Fabrication Research and Education (CAFÉ) program (GR129846) and TNI-OSU/IMR Catalyst Funding (GR137976).

Author contributions

M.M. designed the structures and performed fabrication, optical microscopy, and IV- & CV- based device characterization, analysis of all diodes, and wrote the manuscript. S.M. and D.P. performed device radiometric characterization and analysis. N.G. grew the absorber material. P.M. performed the electron microscopy and analysis. F.K. performed the CV measurement of PIN diodes. Y.X. helped with initial

fabrication and CAD figure design. S.A. and S.K. helped with data analysis and supervised the entire project. All authors approved the manuscript.

Supplementary Files

This is a list of supplementary files associated with this preprint. Click to download.

- HeterogeneouslyIntegratedGaAsSbSiSACMSupplementaryInformation.docx